ATTEMPT TO MEASURE BUILDING DEFORMATION USING CRACK DISPLACEMENT TRANSDUCERS

Y. Okayasu*, High energy accelerator research organization (KEK), Tsukuba, Japan

Abstract

Since 2020, we have been continuing to conduct the control survey of the KEK e^-/e^+ injector linac in Tsukuba campus using a laser tracker and digital level. Trends of our survey data suggest unique displacements in the accelerator equipment coordinates.

The causes of the displacements are considered to be 1) the lack of constrains in network analysis in surveying the injector linac, which is one-path, compared to ring-type accelerators such as storage rings, and 2) displacements in the injector linac building, which consists of multiple blocks.

To first confirm whether the building is actually moving or not, we experimentally introduced crack displacement transducers at one point on the building construction boundary in February 2023 and began a demonstration test to evaluate building movement.

INTRODUCTION

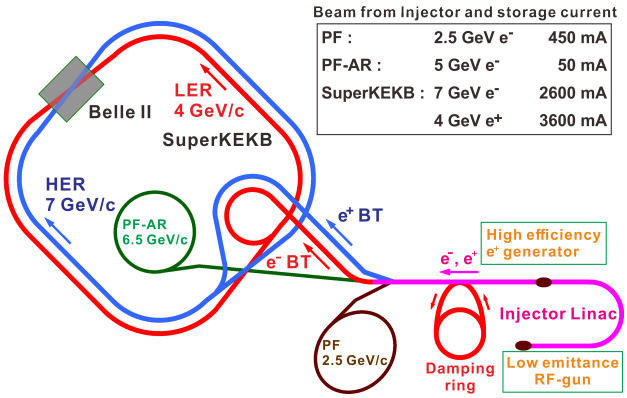

Figure 1: Schematics of the accelerator complex and their own beam energies and currents in the KEK Tsukuba campus.

The main accelerators installed at KEK Tsukuba Campus are summarized in following four accelerators; SuperKEKB, specialized for high-energy elementary particle physics experiments; Photon Factory (PF), the first X-ray light source developed in Japan; Photon Factory Advanced Ring (PF-AR), a light source accelerator modified from the front accelerator of TRISTAN; and the injector linac that supply electron and positron beams to these ring accelerators as described in Fig. 1. In addition to these above, the compact Energy Recovery Linac (cERL) and KEK Education and Training Accelerator (KETA), which specializes in educating students, faculty, and corporate engineers, are also in operation. In SuperKEKB, electrons and positrons orbit the High Energy Ring (HER) and Low Energy Ring (LER), respectively. Both electrons and positrons collide at the interaction point and the scattered particles are finally detected by the Belle II detector.

Among these, SuperKEKB has set the challenging goal of reaching an electron-positron collision luminosity of the order of 10^{35} $cm^{-2}s^{-1}$, and is working to reduce the emittance and stabilize the beam in both the injector linac and SuperKEKB HER and LER rings. As part of this, we are working to improve the alignment accuracy of accelerator equipment, and in 2020 we introduced the control survey and network analysis of the entire injector linac using a laser tracker and digital level [1].

The injector linac (645-m long in total) consists of 9 sectors, which are defined from the upstream as Sectors A, B, J-arc, C and 1–5, as shown in Fig. 2. The electron beam for positron generation is generated by a thermal electron gun, and the other electron beams are generated by an RF photo-cathode electron gun. After passing through Sectors A and B (125 m), the electron beams are turned 180° in J-arc (36 m). Of these, positron beam is generated at a tungsten target located in Sector 1 and reduced its emittance through a damping ring and passed through Sectors 3–5. Other electron beams are passed through Sectors C–5 (484 m). Eventually, all beams are supplied to each of the ring accelerators shown in Fig. 2.

Each sector is equipped with unit girders that support accelerating tubes, electromagnets, diagnostic equipment, and vacuum equipment. Quadrant photo-diode sensors (QPDs) are mounted on both ends of the unit girder. Two He-Ne light sources are installed at the beginning of Sector A and Sector C, and the unit girders of the long straight sections, Sectors A–B and C–5, are precisely aligned using the coordinates of the laser baseline measured by the QPDs [2].

CONTROL SURVEY

The conventional control survey with the laser tracker (Leica AT-401) and digital level (Trimble DiNi0.3) has been demonstrated every summer for all magnets, monuments on the wall and floor, and unit girders in the injector linac since 2020. The number of units, magnets, and monuments for each sector are listed in Table 1. Typical accuracies of the laser tracker and digital level for the control survey in the injector linac are summarized in Table 2.

Spacial intervals and number of station points of the laser tracker and digital level are ~10 m, 62 points and ~16 m, 21 points (total 43 points : round-trip), respectively. Especially for the level survey, we demonstrate the round-trip survey and apply a loop-closure correction for the level data. The control survey and network analysis are demonstrated with

* okayasu@post.kek.jp

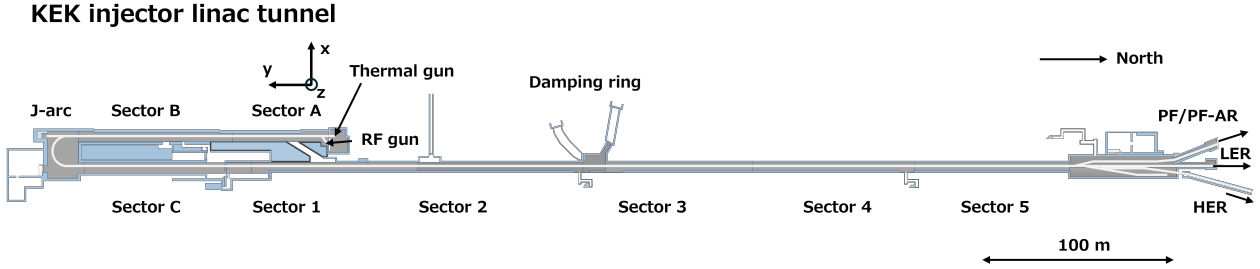

Figure 2: Schematic view of the KEK injector linac. Sector names and the coordinate definition of the network analysis are also overlaid.

Table 1: Summary of length, number of units, magnets, and monuments on each sector.

Sector name	A	B	J-arc	C	1	2	3	4	5
Length [m]	48.0	76.8	36.1	81.6	83.3	92.9	69.9	79.5	76.8
# of units	4	8	1	8	7	7	8	8	8
# of magnets	65	14	35	18	74	90	20	16	34
# of monuments	15	19	10	21	32	32	17	19	20

Table 2: Evaluated typical accuracies of the laser tracker and digital level for the control survey in KEK injector linac.

Leica AT-401	
Horizontal angle	2.7 ± 1.1 μrad
Vertical angle	2.5 ± 1.0 μrad
Distance	$18.9^{+14.3}_{11.0}$ μm
Trimble DiNi0.3	
Level	4.7 μm

Spatial Analyzer (SA, New River Kinematics). The level survey is controlled by Microsoft VBA macro through a Bluetooth connection between the digital level and a computer. The network analysis is demonstrated by SA with weighted and the loop-closure corrected level data. In the network analysis, the weight factor of the digital level is assigned a factor of ∼3 so that the measurement error is 4.7 μm as shown in Table 2, and all other laser tracker data was left at the default value of 1.

The coordinate system definition is as follows; the origin is set on a magnet (PX_A1_M) center which is located on the beam level at Sector A. y-axis is defined with PX_A1_M and an another magnet (QD_B7_4) which is located at the most downstream of Sector B. x-axis is orthogonal to y-axis on the beam level plane and z-axis vertical as shown in Fig 2.

Fig. 3 compares x (*upper*) and z (*lower*) components surveyed on 2020 (◯), 2021 (△), and 2023 (□) of all magnets along the path length. Positions of expansion joints are also overlaid as dotted lines and hatching and sector IDs are also overlaid. The y coordinate of the beam direction component is less important than the x and z components, thus it is not discussed in this paper. Note that, for the 2022 data, the loop closure correction result of the digital level survey was ∼0.45 mm, significantly worse than in previous years (< 0.3 mm), and was not suitable for weighted network analysis, so analysis was abandoned.

In Fig. 3 (*upper*), the vertical axis, Δx is the residual between measured and designed coordinates $\Delta x = x_{\rm meas} - x_{\rm des}$. Note that, Δx in J-arc are not displayed, and in Sectors C–5, Δx is subtracted by -15000 mm, which is corresponding to a designed distance from Sectors A–B and C–5, in order to represent data in one scale. It is found that the gradient of Δx in Sector C–5 increases over the years, where the gradient of ∼0.1 μrad beyond the J-arc exit was recognized at the construction phase. Especially at the end of Sector 2, where the crack displacement transducers are installed, Δx evaluated from 2020, 2021, and 2023 survey data are 18.19, 18.21, and 19.76 mm, respectively. This is considered to be due to 1) the accumulation of analysis errors in the network analysis, and 2) the injector linac building itself fluctuating around the expansion joint. On the other hand, the level data (z) shown in Fig. 3 (*lower*) has a maximum value near the J-arc, however this is distribution before applying a geodetic line correction.

The geodetic line correction is introduced and applied to the level data z in order to transfer the survey data to the beam analysis and 3D model control in a Computer Aided Design (CAD) environment, which require absolute coordinates with respect to an idealistic single plane. Even if the geodetic shape of the earth is assumed to be completely spherical with a radius curvature of $r = 6371 \times 10^3$ m, the elevation difference ΔH for a straight line of $L = 500$ m is estimated to be

$$\Delta H = r(1 - \cos\theta) \simeq 5 \ \text{[mm]}, \quad (1)$$

$$\theta = \sin^{-1}\left(\frac{L}{2r}\right), \quad (2)$$

where θ is estimated to be ∼39 μrad for $L = 500$ m. In general, a network survey is performed by moving its station points along the geodetic curve.

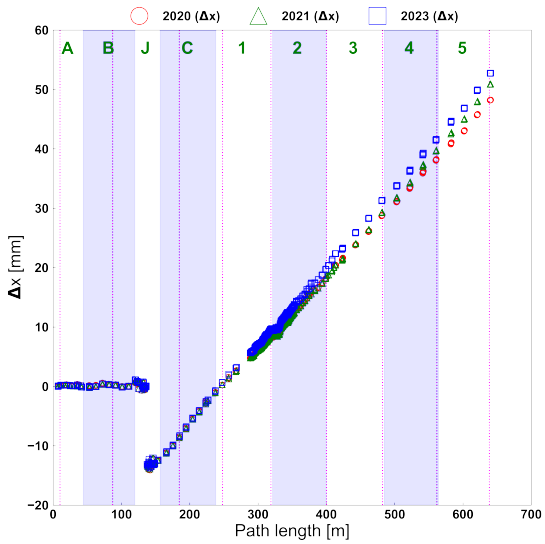

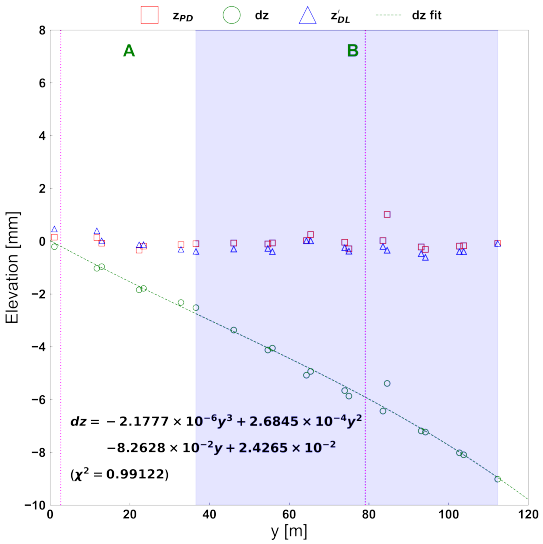

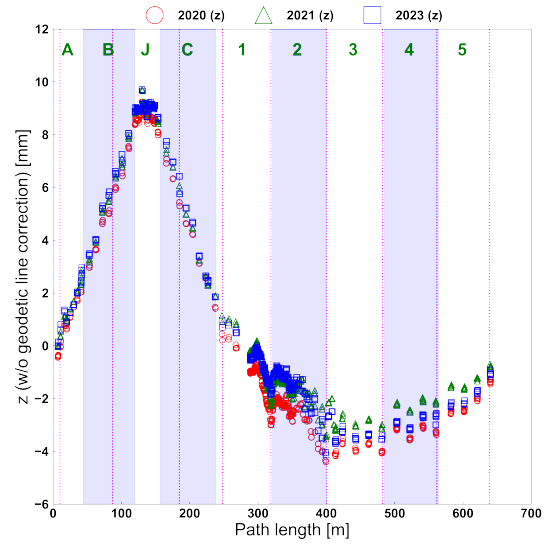

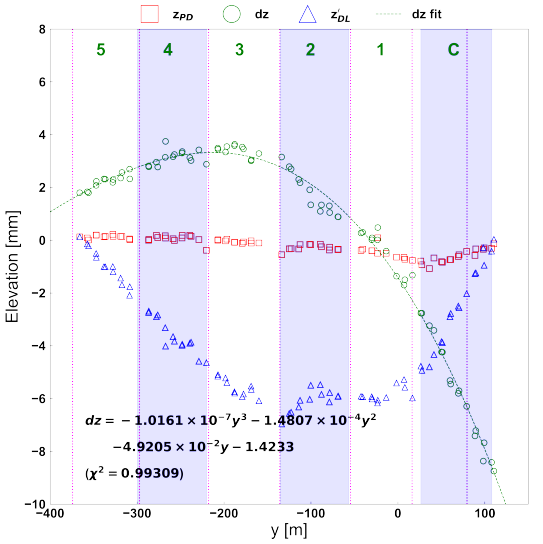

Figure 3: x (*upper*) and z (*lower*) coordinates distributions derived by the control survey and network analysis and comparison between 2020 (◯), 2021 (△), and 2023 (□) data. For the vertical axis, Δx is the residual form the designed coordinate $\Delta x = x_{\mathrm{meas}} - x_{\mathrm{des}}$. Horizontal axes are path length of fiducial point orientations. Hatched areas distinguish each sector and vertical dotted lines represent locations of expansion joints among building blocks.

Figure 4: Measured QPD elevation z_{PD} (□) and residuals of the elevation dz (◯). Values of slope adjusted z'_{PD} (△) are also plotted for both sectors A–B (*upper*) and C–5 (*lower*). Fittings with third polynomial functions (dZ_{fit}) are also overlaid with dashed lines for each histogram. Elevation data were surveyed in 2023 with the digital level.

Therefore, a level network survey for any components on a long straight line, such as linacs over 50-m long, is required to apply the geodetic line correction, where ΔH exceeds a few tens of micrometers, a value equivalent to the typical measurement accuracy of laser trackers.

Two elevation data sets; a laser QPD (z_{PD}) and a leveling survey with the digital level (z_{DL}) for the geodetic line correction in the injector linac.

Before the QPD measurements for both straight lines in Sectors A–B and C–5, tilt adjustments were made for each laser injection point as their pointings were located at the centers on both ends of the QPDs. Each QPD housing has an arm structure with its fiducial point, whose level is equivalent to the QPD center.

These fiducial points are used in the network survey with the laser tracker and digital level. Since the QPD measurement system's operation ceased in 2019 due to a fire incident, we separately used past data sets for the QPD measurements;

Sectors A–B measured in 2018 and Sectors C–5 in 2016. z_{PD} (□), z_{DL}, and their residuals dz (◯) are related by

$$dz = z_{PD} - z_{DL} \tag{3}$$

and shown in Fig. 4 for Sectors A–B (*upper*) and C–5 (*lower*).

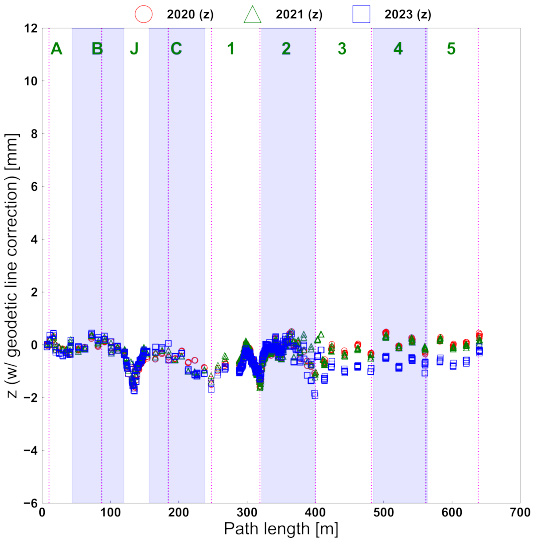

Figure 5: z-coordinate distributions derived by network surveys in 2020 (◯), 2021 (△), and 2023 (□). Geodetic line corrections are also applied for both years' data.

In addition, the z_{DL} distribution is corrected as its start and end elevations correspond to those of z_{PD}, which are also plotted as z'_{DL} (△). The maximum difference of elevation (z'_{PD}) in Sectors C–5 (L ≃ 500 m) is estimated to be 6.4 mm, which equals to 5 mm in a rough calculation with Eq. (1).

The elevation residuals described in Eq. (3) are individually fitted with third polynomial fitting functions (dz_{fit}) of y coordinates for each survey year in both Sectors A–B and C–5. Corrected elevations z_{cor} are finally derived as

$$z_{cor} = z_{DL} + dz_{fit}. \tag{4}$$

The corrected elevations z of all the magnet surveyed in 2020, 2021, and 2023 are compared in Fig. 5. Comparing to the case without the geodetic line correction as shown in Fig. 3 (*lower*), the maximum elevations of ~9 mm at J-arc and the minimum elevations of ~4 mm at the boundary between Sectors 2 and 3 were reduced, and the deviations of the elevation converged within -1.6 mm to 0.5 mm after applying the correction to the elevation for each year.

Coordinate uncertainties of horizontal x (*upper*) and vertical z (*lower*) are evaluated by the network analysis for 2020 (◯), 2021 (△), and 2023 (□) years and compared along the path length in Fig. 6. Uncertainties of x has characteristic distributions and trends compared to such storage rings

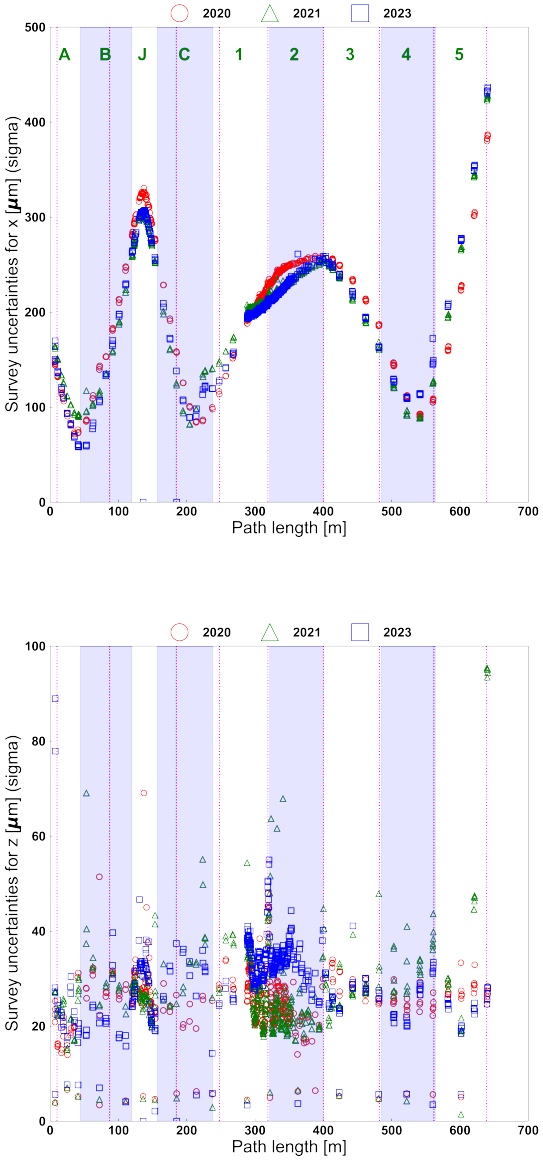

Figure 6: Survey uncertainties of horizontal x (*upper*) and vertical z (*lower*) component comparison between 2020 (◯), 2021 (△), and 2023 (□) evaluated by the network analysis. The horizontal axis is path length in meters. Sector regions are represented with hatching and the locations of expansion joints are shown with vertical dotted lines.

as SPring-8, where the distributions are monotonously periodic for the entire circumference [4]. Variations of the uncertainty x along the path length show remarkable peak structures at J-arc, and at Sectors A–B and 1–3 for each survey year. The slope shape of uncertainty x in Sector 1–2 of 2021 and 2023 survey is different from that of 2020 survey due to the addition of a station point at the bypass line that connects Sectors A and 1. In Sector 5, uncertainty x increases monotonically year by year. It is considered to be numerical analysis error that is also well-reproduced by

simulations [1]. Uncertainty z is almost equal through the entire path length. The intermittent uncertainties z of ~5 μm are the result of adjusting the weight factor of the digital level data in the network analysis so that the uncertainty z is 4.7 μm, as mentioned above.

CRACK DISPLACEMENT TRANSDUCERS

In order to determine whether the displacement at the end of the injector linac was due to fluctuations at expansion joints or due to analytical errors in the network analysis, crack displacement transducers (KG-2A, Tokyo Measuring Instruments Laboratory Co., Ltd. [3]) were experimentally installed at the end of Sector 2 in January 2024. The measurement principle of KG-2A is a load cell that detects strain.

Table 3: Main specifications of the crack displacement transducer KG-2A

Capacity	±2 mm
Rated output	Approx. 1.5 mV/V (3000×10^{-6} strain)
Sensitivity	1500×10^{-6} strain/mm
Non-linearity	0.5% RO
Spring force	15 N
Temperature range	-20 to +60 °C
Weight	180 g

A schematic drawing of KG-2A setups installed at the expansion joint of Sector 2 and 3 and a configuration of the building movement monitoring system for the injector linac is described in Fig. 7. The material used for the support mechanism of KG-2A is invar, which has an extremely low thermal expansion coefficient. Note that, the radiation shield housing for KG-2As are not displayed in Fig. 7 (*upper*) for clarity. Three KG-2A units are installed on the floor of the accelerator tunnel, stradding the construction boundary. They monitor displacements in the west-east (x), north-south (y), and up-down (z) directions, respectively. Communication of voltage information associate with the displacements and power supply are carried out via a network module (NSW-014C [3]). Voltage data is converted into displacement information by a handheld measuring device (TC-35N [3]) installed in the klystron gallery. TC-35N also provides electric power to both KG-2A and NSW-014C. Measurement and data acquisition commands are remotely controlled via a Raspberry Pi, and the acquired data is stored in a database. The main specifications of KG-2A are listed in Table 3.

KG-2A itself has a protection rating equivalent to IP65, however since the KG-2A and NSW-014C is installed in a radiation environment, they are protected by a housing made of boron-doped polyethylene and lead sheeting.

Trends of displacement in x (west − east), y (north − south), and z (up − down) directions at the expansion joint between Sectors 2 and 3 are shown in Fig. 8. As shown in Fig. 8, the displacements of the expansion joint over a period of five months were -54 < x [μm] < 8, -346 < y [μm] < 63, -49 < z [μm] < 80. Fluctuations seen in the distribution of each component, especially in the y-direction component, are due to the day-night difference in room temperature.

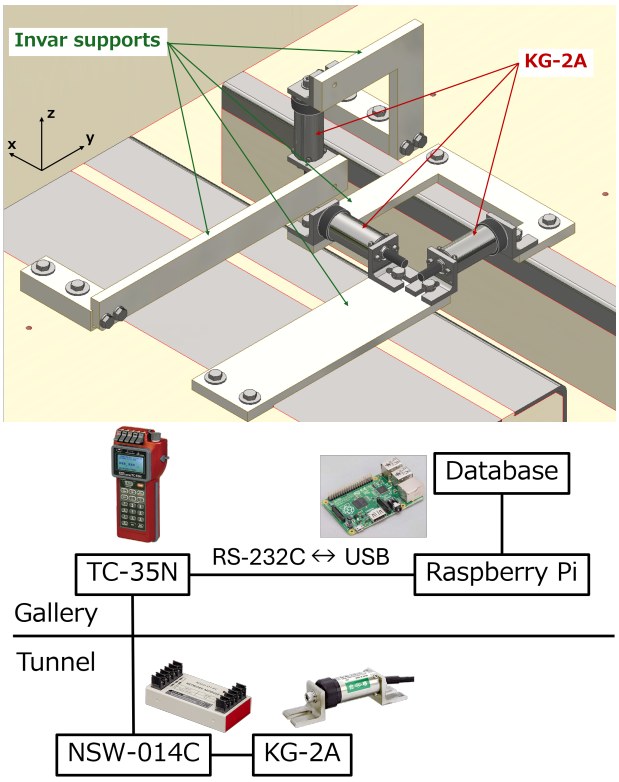

Figure 7: Schematics of KG-2A setups installed at the expansion joint of Sector 2 and 3 (*upper*) and a configuration of the building movement monitoring system for KEK injector linac (*lower*).

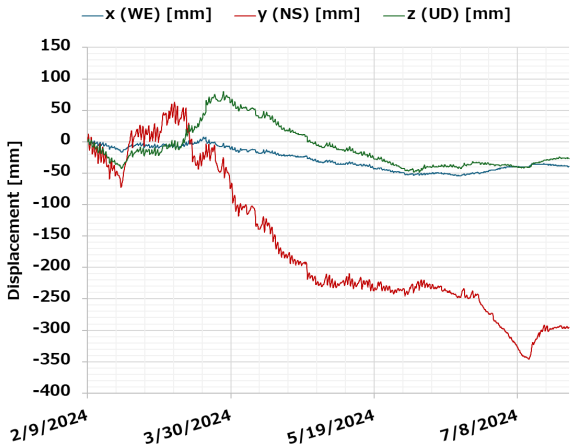

Figure 8: Trends of displacement in x (west − east), y (north − south), and z (up − down) directions at the expansion joint between Sectors 2 and 3.

DISCUSSION

Although there are fluctuations depending on the temperature coefficient, it seems possible to measure building movements using the crack displacement transducer.

As discussed with Fig. 3 (*upper*), the differences Δx between the measured and designed values of the horizontal x coordinates at the expansion joint of Sectors 2 and 3 in 2020, 2021, and 2023 were 18.19, 18.21, and 19.76 mm, respectively, with the variation range of the three surveys being 1.57 mm. On the other hand, the displacement of x over a five month period measured by the crack displacement transducer installed at the expansion joint of Sectors 2 and 3 was -54 < x [μm] < 8. Survey data indicates that the end of Sector 2 has moved 1.57 mm to the west over a three-year period, while crack displacement transducer data indicates that the expansion joint has widened by 8 μm and shrunk by 54 μm in the east-west direction over a five-month period.

Since the measurement period is short, the validity of the survey data cannot be directory confirmed by crack displacement transducers data. In order to verify the validity of the displacement, it is necessary to set up crack displacement transducer systems at least in two or three more locations downstream from the end of Sector 2 and collect longer-term displacement trend data.

On the other hand, in the control survey, as shown in Fig. 6 (*upper*), the uncertainty of the horizontal coordinate x has a unique distribution. Therefore, it is necessary to make the uncertainty distribution as uniform as possible, like the case of storage rings, by introducing a weight factor, which is currently applied only to digital level data in network analysis, to the laser tracker data as well, normalized by the number of control points surveyed per station point.

SUMMARY

The conventional control survey using the laser tracker and digital level and the network analysis were conducted at KEK injector linac since 2020. A unique displacement trend in the east-west (x) direction was observed from Sector 2 onward. Possible causes of the displacement are 1) accumulation of numerical errors in the network analysis, and 2) movement of the building housing the injector linac.

To verify the latter possibility, crack displacement transducers were installed at the expansion joint at the end of Sector 2 as a trial in January 2024 and movement monitoring began.

Although fluctuations depending on the temperature coefficient are found in displacement distributions, it seems possible to measure building movements using crack displacement transducers. It is necessary to install the systems at least in two or three more locations downstream from the end of Sector 2 and collect long-term displacement trend data in order to verify the validity of the displacement measured by the control survey.

REFERENCES

[1] Y. Okayasu *et al.*, Rev. Sci. Instrum., **94**, 075107 (2023). doi:10.1063/5.0155651.

[2] Y. Okayasu *et al.*, "Control survey for KEK e^+/e^- Injector Linac" in Proceedings of 16th International Workshop on Accelerator Alignment (IWAA2022), Ferney-Voltarie, France, 2022.

[3] Tokyo Measuring Instruments Laboratory Co., Ltd., https://tml.jp/e

[4] Y. Okayasu *et al.*, J. Instrum.. **15**, P03033 (2020), doi:10.1088/1748-0221/15/03/P03033